LAND COVER CLASSIFICATION OF KUMAMOTO, JAPAN USING POLARIMETRIC DECOMPOSITION OF PALSAR-2 DATA

Homa Zakeri[1], Fumio Yamazaki[2], Wen Liu[3]

[1]Graduate Student, Chiba University, Chiba, Japan. Email: homa.zakeri@chiba-u.jp
[2] Professor, Chiba University, Chiba, Japan. Email: fumio.yamazaki@faculty.chiba-u.jp
[3] Assistant Professor, Chiba University, Chiba, Japan. Email: wen.liu@chiba-u.jp

KEY WORDS: Land cover classification, SAR imagery, decomposition, 2016 Kumamoto earthquake

ABSTRACT: Polarized SAR images have been extensively used recently for monitoring urban and suburban areas. Since different polarizations represent different scattering coefficients of the same target, they can be used to prepare land cover maps, which contain vital information for several fields, such as environmental science, seismic risk assessment, urban management and planning. SAR amplitude data have been used mostly for obtaining the ground surface information whereas phase data can provide more information of the ground objects. Therefore, in this research, full polarized data of ALOS-2 PALSAR-2 with 5.13-m resolution in an ascending path were used to classify various land covers in Kumamoto, Japan. Accordingly, the Yamaguchi-4 decomposition was applied on the polarimetric dataset of the study area. Since the Yamaguchi-4 decomposition provides surface, volume, double bounce, and helix scatterings, it can be effective for classifying not only natural objects on the ground but also for man-made structures with different orientations. The Support Vector Machine (SVM) algorithm was used for supervised classification by the Yamaguchi-4 decomposition. The confusion matrix with the kappa coefficient, overall-, producer-, and user-accuracies were prepared for the classification results to be compared with the truth data. This research aims to explore the potential of the decomposition method for classifying various land covers of urban and suburban areas.

1. INTRODUCTION

Remote sensing data have been used widely in recent decades for monitoring and detecting manmade and natural objects on the ground (Moya et al., 2017; Lacerda et al., 2016; Immitzer, 2012; Zakeri et al., 2016). Land cover classification is an essential part of remotely sensed image analysis because it provides vital information in several applications such as urban planning, seismic risk assessment, ecological and urgent environmental monitoring in regional and global scales (Colaninno et al., 2012; Molch, 2000; Rathje and Adams, 2008; Yamazaki et al., 2011; Liu et al., 2013; Yamazaki and Liu, 2014). Remote sensing data provided by optical sensors have been commonly used for classification of various land covers such as different types of vegetation, urban, suburban, wetland, soil, and etc. But optical remote sensors are dependent on weather and time conditions. Therefore, there is a limitation for capturing optical images especially in emergency situations or for tropical regions.

Several studies have been conducted using radar remote sensing and provided high accurate results. Nakmuenwai et al. (2017) extracted the inundated areas using multi-temporal dual polarized RADARSAT-2 images for the 2011 central flood of Thailand. Liu and Yamazaki (2017) used multi-temporal PALSAR-2 images to detect collapsed buildings in the 2016 Kumamoto, Japan, earthquake. Bahri et al. (2015) used pre- and post-event images of ALOS-2 for damage assessment of the 2015 Nepal earthquake. Zakeri et al. (2017) conducted land cover classification of Tehran using dual polarized ALOS-2 and Sentinel-1 images.

ALOS-2 SAR products were chosen to use in this study. Advanced Land Observing Satellite 2 (ALOS-2) was launched on 24 May 2014 with an enhanced L-band SAR sensor, Phased Array type L-band Synthetic Aperture Radar-2 (PALSAR-2). It can capture images in right and left path directions. One of the objective of ALOS-2 is updating of land covers. ALOS-2 images have been used in several studies for land cover classification with high accuracy results (Mi et al., 2014; Walker et al., 2010). In this study, we used full polarimetric (HH, HV, VV, VH) images of ALOS-2, which were taken on August 11, 2016 for classifying various land covers of Kumamoto, Japan.

The Kumamoto prefecture was the most severely affected area in the 2016 Kumamoto earthquake. The Kumamoto earthquake was a series of earthquakes including Mw 7.0 main-shock on April 16, 2016 at 16:25 (UTC) or 01:25 (JST), and the Mw 6.2 foreshock on April 14, 2016 at 12:26 (UTC) or 21:26 (JST). The earthquake sequence caused significant damage to buildings, infrastructures, and road networks. The number of casualties was 50 due to direct causes and the number of evacuees at the peak of the earthquake was about 200 thousands according to the report of the Japanese Red Cross, published on 17 May 2016 (USGS, 2016; Japan Red Cross, 2016). Several studies have been conducted after the 2016 Kumamoto earthquake on the affected area (Goken et al., 2017; Liu and Yamazaki, 2017) to

detect the changes and damaged areas.

In this study, we used a decomposition method to achieve better backscattering characteristics of the ground objects using the ALOS-2 full polarimetric dataset. This methodology, which is known as target decomposition, provides physical and geometrical properties of the ground surface. Indeed, it separates the objects' scattering matrix into individual components that are related to respective scattering mechanisms (Cloude, 1997). Therefore, we can obtain more information on land cover classification. The Yamaguchi-4 decomposition (Yamaguchi et al., 2005) is selected since it includes four different components, such as double bounce, surface, volume, and helix, which can represent the scattering mechanism of different ground objects including urban structures. Then the Support Vector Machine (SVM) classification was applied on the result of the decomposition and the result was compared with the classification map prepared by JAXA.

2. THE STUDY AREA AND DATASET

The study area of this research is located in Kumamoto, Japan as shown in **Figure 1**, which is placed above the Futagawa fault. The study area was selected for this research because it contains a part of Kumamoto city and Mashiki town which were severely affected by the 2016 Kumamoto earthquake. Also this area includes various land covers that can be used to test the methodology of this study for the purpose of land cover classification.

A full polarimetric dataset of ALOS-2 PALSAR-2 was used for the analysis in this study. The full polarized image of ALOS-2 was taken on August 11, 2016 in the strip map mode, with the incident angle of 33.86º at the center of the image, and the spatial resolution of 5.13 m. The SAR images were provided as the range and single-look azimuth compressed data with the processing level 1.1, which is represented by the complex I and Q channels to preserve the amplitude and phase information. The objective of this study is to use phase information of SAR images for land cover classification of the study area. Therefore, the pre-processing for the phase dataset including four methods were applied on the ALOS-2 full polarized images. The first step of pre-processing includes preparation of the coherency matrix, T_3. Therefore, the scattering matrix, *S*, which represents polarimetric SAR measures based on the horizontal (H) and vertical (V) polarizations, is shown as:

$$S = \begin{bmatrix} S_{hh} & S_{hv} \\ S_{vh} & S_{vv} \end{bmatrix} \tag{1}$$

For a monostatic backscattering case, the target vector becomes:

$$k = \frac{1}{\sqrt{2}} \left[S_{hh}, S_{vv}, S_{hh} - S_{vv}, 2S_{hv} \right]^T \tag{2}$$

The 3x3 coherency matrix, T_3, is given by:

$$T_3 = kk^H \tag{3}$$

where *H* represents the transpose conjugate. The resulting T_3 has nine independent elements.

Then, the refined Lee filter of window size 13×13 with the number of looks equal to one was applied on the dataset to remove speckle noise of the images. The number of the look of SAR data was used to estimate the standard deviation of the speckle noise. Afterward, orientation angle correction was applied on the dataset to make the horizontal polarization parallel to the ground terrain slope. Geometric correction using the range Doppler orthorectification method was used to represent the data geometrically similar to the real world. The Shuttle Radar Topography Mission (SRTM) data were introduced as one arc-second (approximately 30-m resolution) digital elevation model (DEM).

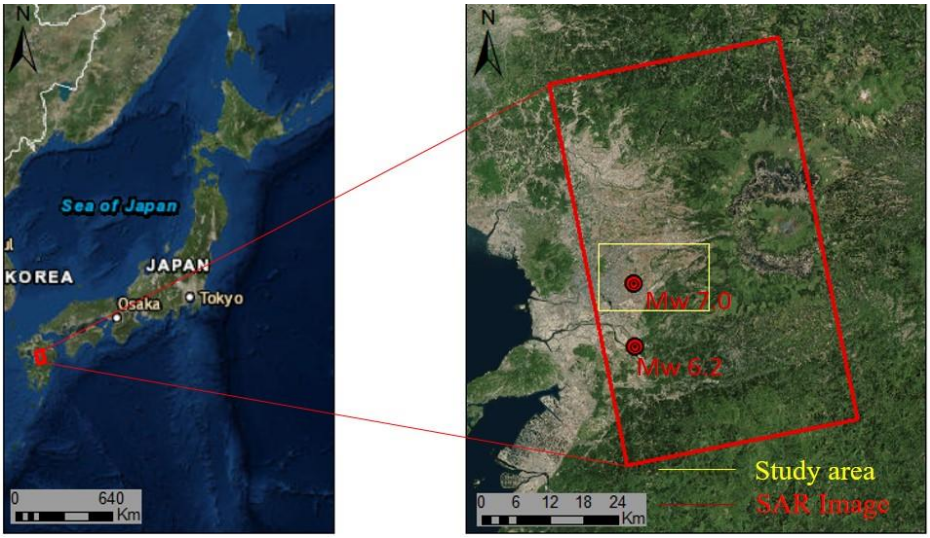

Figure 1 The location of the study area (yellow frame) and SAR datasets (red frame).

3. METHODOLOGY

The overall framework of this study is shown in **Figure 2.** This framework contains five steps: pre-processing, Yamaguchi-4 decomposition, layer stacking of decomposition values, supervised classification (SVM), and accuracy assessment. After pre-processing, the polarimetric decomposition was used to introduce the physical characteristics of objects on the ground. The decomposition methods, which produce various scatterings such as surface, volume, double bounce, helix, wire, etc., can provide more information from different properties on the ground with different orientations, materials, and structures. Therefore, the use of decomposition methods would be sufficient for classifying an area with different land covers. Since the objective of this study is land cover classification of urban and suburban areas including various man-made structures and natural land covers, the Yamaguchi-4 decomposition with the capability of preparing double bounce, volume, surface, and helix scatterings was selected. The double bounce scattering represents man-made objects such as built-up areas. The volume scattering illustrates vegetation and buildings in different orientations with respect to the radar illumination. The surface scattering demonstrates bare soils, crop lands, snow, and volcano ashes. The helix scattering represents complicated man-made structures.

The previous approaches have used the reflection symmetry condition, which introduces the covariance between the backscatter HH, and the conjugate of the backscatter HV is close to zero as follows:

$$\left\langle S_{HH} S^{*}{}_{HV} \right\rangle \approx 0 \tag{4}$$

$$\left\langle S_{VV} S^{*}{}_{VH} \right\rangle \approx 0 \tag{5}$$

Thus, from the covariance matrix, the four components, which are shown in black frames, becomes zero as follows:

$$\left\langle [C] \right\rangle^{HV} = \begin{bmatrix} \left\langle |S_{HH}|^2 \right\rangle & \boxed{\sqrt{2}\left\langle S_{HH} S^{*}{}_{HV} \right\rangle} & \left\langle S_{HH} S^{*}{}_{VV} \right\rangle \\ \boxed{\left\langle S_{HV} S^{*}{}_{HH} \right\rangle} & 2\left\langle |S_{HV}|^2 \right\rangle & \boxed{\sqrt{2}\left\langle S_{HV} S^{*}{}_{VV} \right\rangle} \\ \left\langle S_{VV} S^{*}{}_{HH} \right\rangle & \boxed{\sqrt{2}\left\langle S_{VV} S^{*}{}_{HV} \right\rangle} & \left\langle |S_{VV}|^2 \right\rangle \end{bmatrix} \tag{6}$$

where $\langle\ \rangle$ denotes the total average of data processing and * denotes the complex conjugate.

Then the covariance matrix is decomposed into three components as follows:

$$\left\langle [C] \right\rangle^{HV} = f_s \left\langle [C] \right\rangle^{hv}_{Surface} + f_d \left\langle [C] \right\rangle^{hv}_{double} + f_v \left\langle [C] \right\rangle^{hv}_{Vol} \tag{7}$$

where $\left\langle [C] \right\rangle^{HV}$ corresponds to spatial average of the data, and $\left\langle [C] \right\rangle^{hv}$ denotes the mathematical average calculated

by an integration expression. The f_s, f_d, and f_v stand for the coefficients of surface, double bounce, and volume scatterings.

This model is based on the simple physical scattering mechanism. Although it is a powerful method to investigate natural targets on the ground surface, the reflection symmetry condition is not true in urban areas (Yamaguchi et al., 2005; Yamaguchi et al., 2006; Yajima et al., 2008). To overcome this issue, Yamaguchi et al. (2005, 2006) proposed a new decomposition method. In this method, the reflection symmetry is not considered zero as follows:

$$\left\langle S_{HH} S^{*}{}_{HV} \right\rangle \neq 0 \tag{8}$$

$$\left\langle S_{VV} S^{*}{}_{VH} \right\rangle \neq 0 \tag{9}$$

Therefore, all the nine components of the covariance matrix (3x3) are decomposed into 4 components as follows:

$$\langle [C] \rangle^{HV} = f_s \langle [C] \rangle^{hv}_{Surface} + f_d \langle [C] \rangle^{hv}_{double} + f_v \langle [C] \rangle^{hv}_{Vol} + f_c \langle [C] \rangle^{hv}_{helix} \tag{10}$$

Four different Yamaguchi-4 scatterings are shown in **Figure 3**. **Figure 4** shows the result of Yamaguchi-4 decomposition, where red, green, and blue colors represent the double bounce, volume, and surface scattering. **Figure 5** illustrates four different Yamaguchi-4 decomposition scatterings including surface, volume, double bounce, and helix.

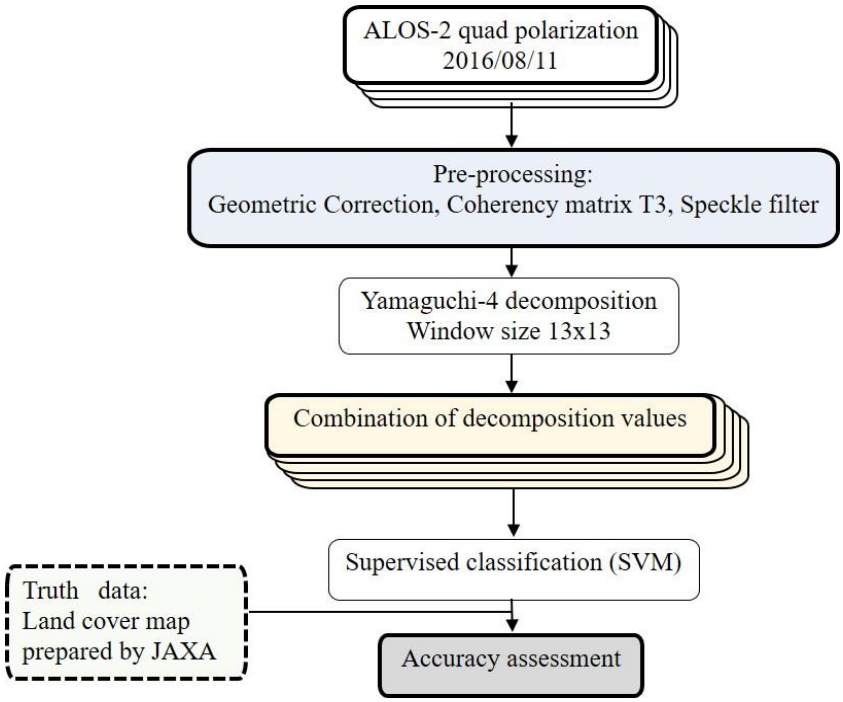

Figure 2 Flowchart of land cover classification using SAR data in this study.

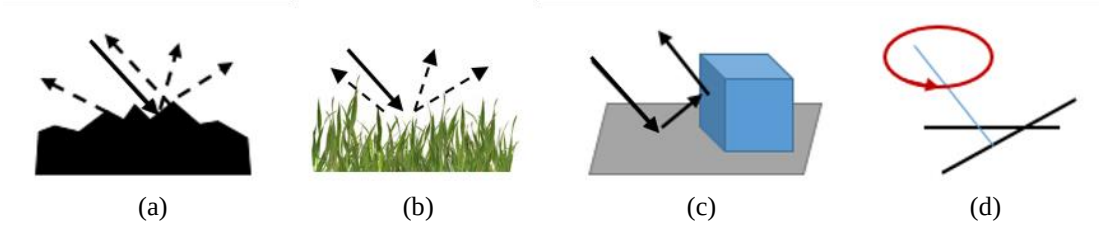

Figure 3 (a) Surface, (b) volume, (c) double bounce, (d) helix scatterings of Yamaguchi-4 decomposition.

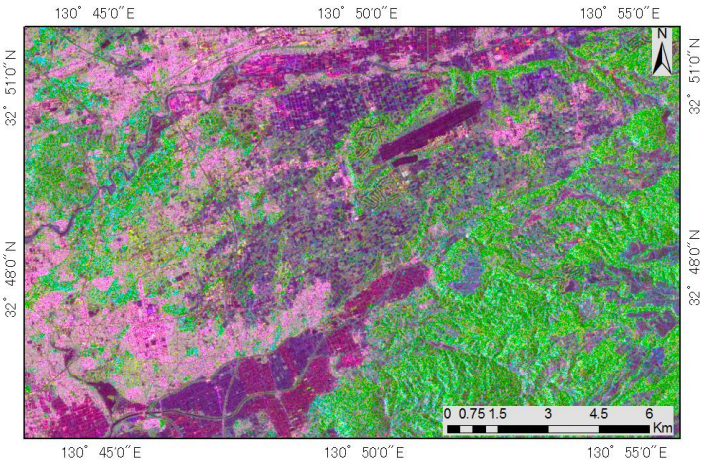

Figure 4 Color composite of Yamaguchi- 4 decomposition with the window size of 13x13 for the study area.

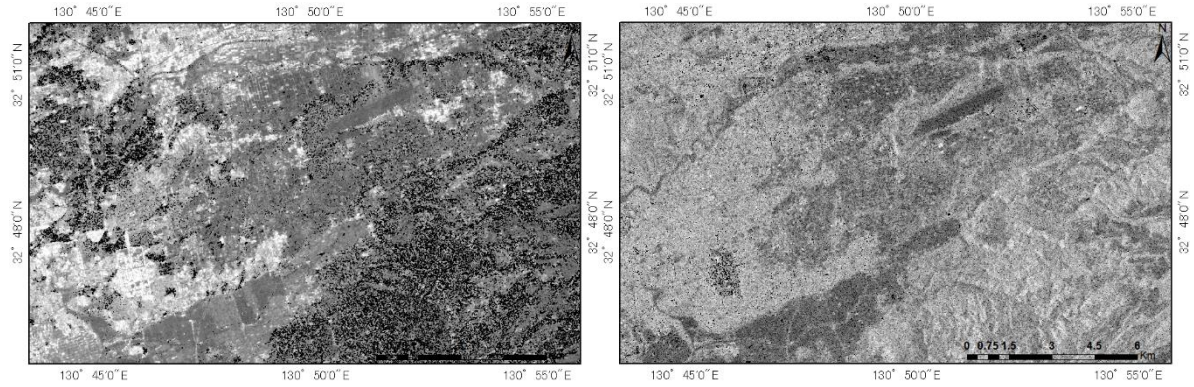

(a) Double bounce scattering

(b) Helix scattering

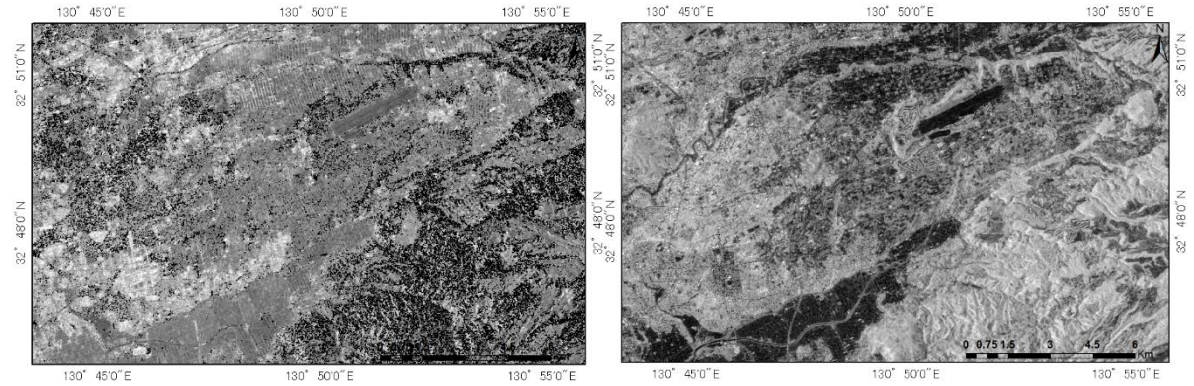

(c) Surface scattering

(d) Volume scattering

Figure 5 Components obtained by Yamaguchi-4 decomposition values with the window size of 13x13.

The SVM algorithm is selected for supervised classification of various land covers in this study. Supervised classification is a training based methodology. In this method, similar pixel values to training samples are classifid and grouped into a considered number of land cover classes (Zakeri et al., 2017). Therefore, selecting training samples is a vital step in this research. After monitoring the study area, seven land covers including bare land, crop and grass, paddy, forest, water, and two different built-up areas were chosen as shown in **Figure 6.** Built-up_1 class is composed of regular Japanese style buildings with gable roofs, and mostly with one to three floors. Built-up_2 class is composed of individual buildings with mostly flat roofs and taller than built-up_1 buildings. Built-up_2 buildings are surrounded by wider roads and open spaces, comparing with those in built-up_1, as shown in **Figure 6.**

The SVM classification was applied on the layer stacking of Yamaguchi-4 scatterings. The radial basis function was used for SVM classification. C and γ are important parameters of this kernel function. The cross-validation was prepared to evaluate the parameter values of C and γ that produce high accuracy classification results. We extracted 7,000 samples (100 per class) randomly. The result of cross-validation shows that values of 10.0 and 0.1 provide the highest accuracy of input data for parameters C and γ, respectively. To check the accuracy of the supervised SVM classification, the confusion matrix was constructed using a land cover map that prepared by JAXA as truth data. This method is a standard way for evaluating classification accuracy in remote sensing (Paneque-Gálvez et al., 2013). The kappa coefficient, overall accuracy, user and producer accuracies were calculated for the confusion matrix.

4. THE RESULT AND DISCUSSION

This study attempts to classify various land covers of the Kumamoto area with high accuracy using the ALOS-2 full polarimetric dataset and an appropriate methodology. The result of SVM classification using the layer stacking of Yamaguchi-4 decomposition values is shown in **Figure 7(a)**.

To assess the accuracy of the SVM classification, the confusion matrix was provided using the truth data. This truth data prepared by the Japan Aerospace Exploration Agency using multi-temporal optical images, which were taken in different seasons (JAXA, 2017). The overall accuracy and the kappa coefficient of 78.0 % and 0.745 were obtained respectively for the JAXA land cover map. The truth data is shown in **Figure 7(b)**, covers the whole target area of this study. This map included four different vegetation types, which have been merged into one vegetation class in this research. Also, crop and grass classes were merged because of the same reason as vegetation class. Since only one urban class is considered by JAXA, two different built-up types, 1 and 2, were merged to make a comparison with the JAXA map as shown in **Figure 7(c)**.

The confusion matrix for the classification result was prepared using the truth data provided by JAXA. The confusion matrix is shown in **Table 1**. The table shows that the overall accuracy and kappa coefficient of 63.29 % and 0.50, respectively. The diagonal elements in this table show the correctly classified pixels in each land cover class. The results of the producer and user accuracies depict that urban and forest classes have the highest accuracies among all the land cover classes. The producer and user accuracies of urban class were 83.57 % and 60.98 %, respectively. Also, the producer and user accuracies of the forest class were 71.98 % and 83.72 %, respectively.

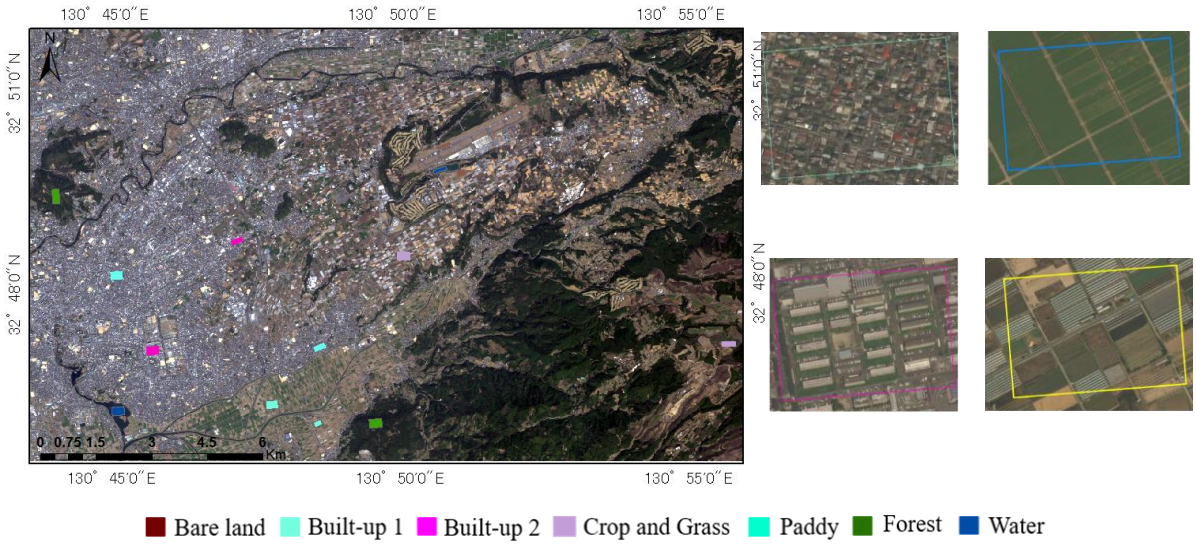

Figure 6 Training samples obtained from ALOS-2 AVNIR-2 of the study area.

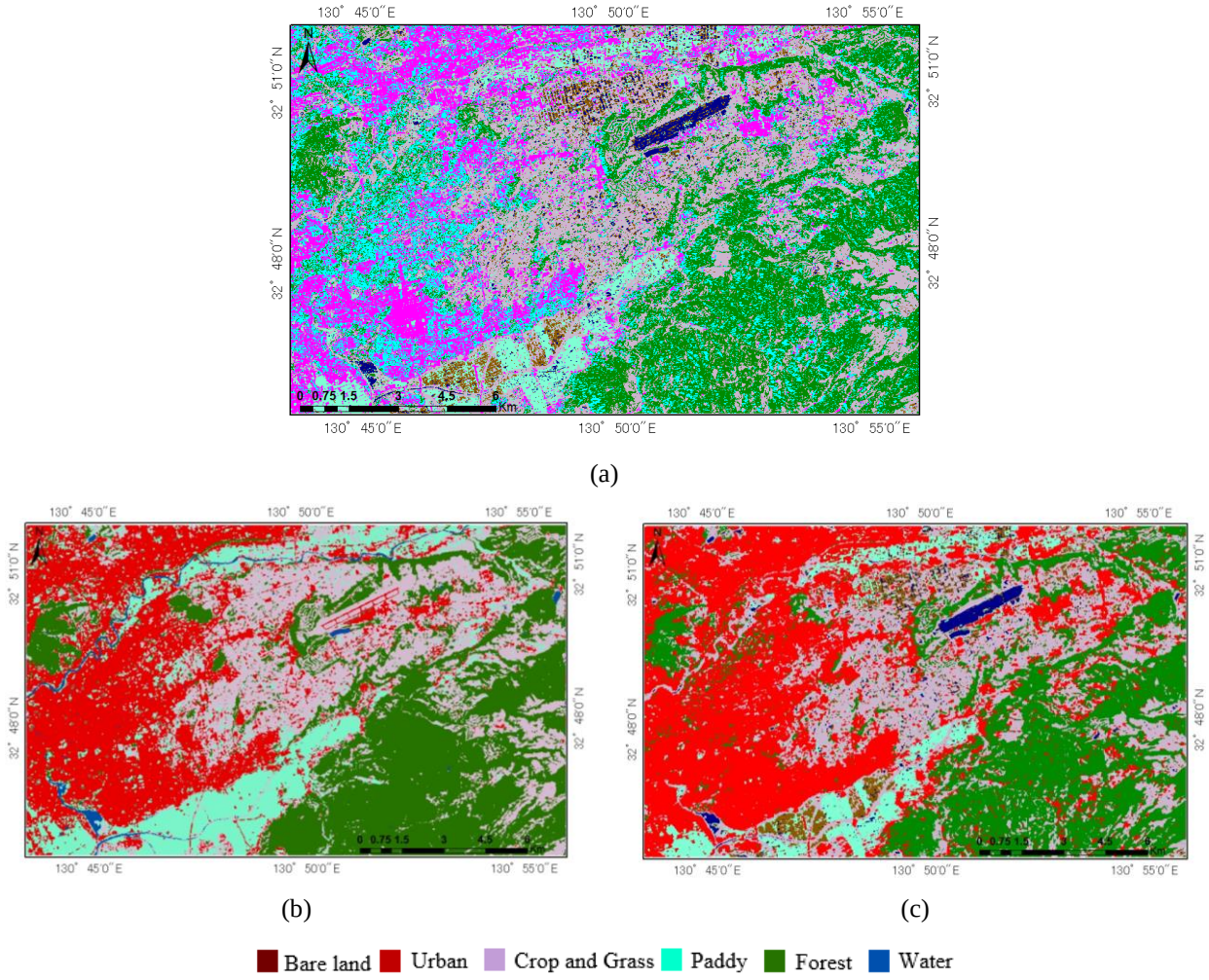

Figure 7 (a) Result of the SVM classification prepared by polarimetric Yamaguchi-4 decomposition values; (b) the land cover map prepared by JAXA, and (c) the cover map created according to the result shown in (a).

Table 1 Confusion matrix of the SVM classification result using polarimetric Yamaguchi-4 values (4 layers).

		Land Cover Classes of Truth Data							**User Accuracy (%)**
		Water	Urban	Paddy	Forest	Crop and Grass	Bare land	Total	
Land Cover Classification from Satellite	Water	19215	17208	22295	448	75434	5097	139697	13.75
	Urban	15559	2026474	332887	299963	611675	36601	3323159	60.98
	Paddy	9887	36194	385912	973	96397	9223	538586	71.65
	Forest	4012	117841	23048	1963263	235034	1744	2344942	83.72
	Crop and Grass	50482	22215	371625	461569	1339463	30139	2475429	54.11
	Bare land	4472	5017	120994	1462	107745	2914	242604	1.20
	Total	103627	2424885	1256761	2727678	2465748	85718	9064417	
Producer Accuracy (%)		18.54	83.57	30.71	71.98	54.32	3.40		**63.29**
Kappa Coefficient 0.50									

5. CONCLUSION

In this research, the Yamaguchi-4 decomposition was applied to an ALOS-2 polarimetric dataset to obtain more information from the SAR image for the purpose of land cover classification. This methodology was selected for improving the supervised classification of SAR images for urban areas. Kumamoto area was chosen as the study area since this area was affected by the 2016 Kumamoto earthquake and needed to be monitored and classified after the event. Full polarized data from L-band ALOS-2 (HH, HV, VV, and VH) were employed and Yamaguchi-4 decomposition values including double bounce, surface, helix, and volume scatterings were prepared. Then SVM algorithm was used for supervised classification of the dataset. Radial basis functions with values 10.0 and 0.1 parameters C and γ, respectively were used. The SVM classification was conducted in seven land covers including bare land, crop and grass, paddy, forest, water, and two different built-up areas (built-up 1 and 2). The result of SVM supervised classification was compared with the land cover map provided by JAXA. The result showed that the Yamaguchi-4 decomposition obtained an acceptable level accuracy. The urban and forest land cover classes showed the highest producer and user accuracies among all the classes.

ACKNOWLEDGMENT

The ALOS PALSAR-2 data used in this study are owned by Japan Aerospace Exploration Agency (JAXA), and were provided through the JAXA's ALOS-2 research program (RA4, PI No. 1503). The Pleiades images are owned by Airbus Defence and Space and licensed to Chiba University.

REFERENCES

Bahri R., Liu W., Yamazaki F., 2015. Damage Assessment of Urban Areas Due to the 2015 Nepal Earthquake Using PALSAR-2 Imagery. The 36th Asian Conference on Remote Sensing, Manila, Philippines, pp. 1-10.

Cloude S.R., Pottier E., 1997. An Entropy Based Classification Scheme for Land Applications of Polarimetric SAR. IEEE Transaction on Geoscience and Remote Sensing, 35, pp. 549-557.

Colaninno N., Roca J., Burns M., Alhadad B., 2012. Defining Densities for Urban Residential Texture, Through Land Use Classification, from LANDSAT TM Imagery: Case Study of Spanish Mediterranean Coast. International Archives of the Photogrammetry, Remote Sensing and Spatial Information Sciences ISPRS Congress, Australia, Vol: XXXIX-B7, 2012XXII, pp. 179-184.

Gokon H., Koshimura S., Meguro K., 2017. Verification of Method for Estimating Building Damage in Extensive Tsunami-affected Areas Using L-band SAR Data. Journal of Disaster Research, 12(2), pp. 251-258.

Japan Aerospace Exploration Agency, 2016. High-resolution Land Use and Land Cover Map. Retrieved September 1, 2017, from http://www.eorc.jaxa.jp/ALOS/lulc/jlulc_jpn.htm

Japan Aerospace Exploration Agency, 2017. About ALOS-overview and Objectives. Retrieved September 1, 2017, from http://global.jaxa.jp/projects/sat/alos/

Japan Red Cross, 2016. Red Cross Responses Keep the Kumamoto Red Cross Hospital Operating. Retrieved September 1, 2017, from https://reliefweb.int/report/japan/japan-kumamoto-earthquake-one-month-report-infographics-17-may-2016

Liu W., Yamazaki F., Gokon H., Koshimura S., 2013. Extraction of Tsunami-Flooded Areas and Damaged Buildings in the 2011 Tohoku-Oki Earthquake from TerraSAR-X Intensity Images. Earthquake Spectra, EERI, 29(S1), pp. S183-S200.

Liu W., Yamazaki F., 2017. Extraction of Collapsed Buildings in the 2016 Kumamoto Earthquake Using Multi-Temporal PALSAR-2 Data. Journal of Disaster Research, 12(2), pp. 241-250.

Lacerda M.P.C., Demattê J.A.M., Sato M.V., Fongaro C.T., Gallo B.C., Souza A.B., 2016. Tropical Texture Determination by Proximal Sensing Using a Regional Spectral Library and Its Relationship with Soil Classification. Remote Sensing, 8(9), pp. 1-20.

Immitzer M., Atzberger C., Koukal T., 2012. Tree Species Classification with Random Forest Using Very High Spatial Resolution 8-band WorldView-2 Satellite Data. Remote Sensing, 4, pp. 2661-2693.

Mi L., Hoan N.T., Tateishi R., Iizuka K., Alsaaideh B., Kobayashi T., 2014. A Study on Tropical Land Cover Classification Using ALOS PALSAR 50 m Ortho-Rectified Mosaic Data. Advances in Remote Sensing, 3, pp. 208-218.

Molch K., 2009. Radar Earth Observation Imagery for Urban Area Characterisation. JRC Scientific and Technical Reports, European Commission: Luxembourg, pp. 1-19.

Nakmuenwai P., Yamazaki F., Liu W., 2017. Automated Extraction of Inundated Areas from Multi-Temporal Dual-Polarization RADARSAT-2 Images of the 2011 Central Thailand Flood. Remote Sensing, 9(1), pp. 1-19.

Paneque-Gálvez J., Mas J.F., Moré G., Cristóbal J., Orta-Martínez M., Luz A.C., Reyes-García V., 2013. Enhanced, 2013. Land Use/Cover Classification of Heterogeneous Tropical Landscapes Using Support Vector Machines and Textural Homogeneity. International Journal of Applied Earth Observation and Geoinformation, 23, pp. 372–383.

Rathje E., Adams B.J., 2008. The Role of Remote Sensing in Earthquake Science and Engineering: Opportunities and Challenges. Earthquake Spectra, 24, pp. 471–492.

United States Geological Survey (USGS), 2016. M7.0-1 km E of Kumamoto-shi, Japan. Retrieved September 1, 2017, from https: //earthquake.usgs.gov/earthquakes/eventpage/us20005iis#executive

Walker W.S., Stickler C.M., Kellndorfer J.M., Kirsch K.M., Nepstad D.C., 2010. Large-Area Classification and Mapping of Forest and Land Cover in the Brazilian Amazon: A Comparative Analysis of ALOS/PALSAR and Landsat Data Sources. IEEE Journal of Selected Topics in Applied Earth Observations and Remote Sensing, 3(4), pp. 594-604.

Yajima Y., Yamaguchi Y., Sato R., Yamada H., Boerner W. M., 2008. POLSAR Image Analysis of Wetlands Using a Modified Four-component Scattering Power Decomposition, IEEE Transactions on Geoscience and Remote Sensing, 46(6), pp. 1667-1773.

Yamaguchi Y., Moriyama T., Ishido M., Yamada H., 2005. Four-component Scattering Model for Polarimetric SAR Image Decomposition, IEEE Transactions on Geoscience and Remote Sensing, 43(8), pp. 1699-1706.

Yamaguchi Y., Yajima Y., Yamada H., 2006. A Four-component Decomposition of POLSAR Images Based on the Coherency Matrix, IEEE Transactions on Geoscience and Remote Sensing letters, 3(3), pp. 292-296.

Yamazaki F., Inoue H., Liu W., 2011. Characteristics of SAR Backscattered Intensity and Its Application to Earthquake Damage Detection. Computational Stochastic Mechanics, pp. 602-606.

Yamazaki F., Liu W., 2014. Urban Change Monitoring: Multi-temporal SAR Images. Encyclopedia of Earthquake Engineering, Springer-Verlag Berlin Heidelberg, pp. 1-13.

Zakeri H., Liu W., Yamazaki F., 2016. Land-Cover Classification of Tehran Using L- and C-band Synthetic Aperture Radar Imagery. The 37th Asian Conference on Remote Sensing, Colombo, Sri Lanka, pp. 1-10.

Zakeri H., Yamazaki F., Liu W., 2017. Texture Analysis and Land Cover Classification of Tehran Using Polarimetric Synthetic Aperture Radar Imagery. Applied Sciences, 7(5), pp. 1-18.